Ultrasonically manufactured space tether

Henri Seppänen

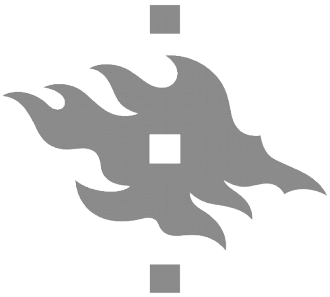

Department of Physics
Faculty of Science
University of Helsinki
March 2015

ACADEMIC DISSERTATION
To be presented
with the permission of the Faculty of Science of the University of Helsinki
for public criticism
in auditorium A132 of the Psychologicum, Siltavuorenpenger 1 A,
on March 10th, 2015, at 12 o'clock noon.

Supervisor

Professor Edward Hæggström
University of Helsinki
Department of Physics
Finland

Reviewers

Associate Professor Michael Mayer
University of Waterloo
Department Mechanical and Mechatronics Engineering
Canada

Dr. Robert P. Hoyt
Tethers Unlimited, Inc.
The United States Of America

Opponent

Prof. Dr.-Ing. Jörg Wallaschek
Gottfried Wilhelm Leibniz Universität Hannover
Institute of Dynamics and Vibration Research
Germany

ISBN978-951-51-0864-7 (paperback)

ISBN 978-951-51-0865-4 (PDF)

Henri Seppänen: Ultrasonically Manufactured Space Tether

Abstract

Tethers are key elements in the electric solar wind sail (E-sail). In this thesis I claim that E-sail tether manufacturing on km scale is possible.

The E-sail is a space propulsion method for interplanetary missions. It uses long, thin and conductive, tethers to create thrust from the solar wind. Based on simulations a full scale E-sail using one hundred 20 km long tethers could create a continuous 1 N thrust. Compared to state of the art ion engines the proposed E-sail produces 10–100 times more specific impulse over the device lifetime. The E-sail is estimated to lower costs of interplanetary missions by reducing the payload mass needed to launch to orbit and by shortening the travel time.

Manufacturing is an important technical challenge to the E-sail. A multifilament tether structure is needed to provide micrometeoroid tolerance to the tether. To address the challenge we combined an industrial ultrasonic wire bonder and a custom-built tether factory for tether production. A customized 3-wire bonding wedge enabled 4-wire multifilament tether manufacturing. The tether comprises 25 and 50 μm in diameter (Ø) aluminum wires that are ultrasonically welded together.

The main result of this thesis is that we showed the feasibility of large-scale device manufacture by producing a continuous 1.04 km long multifilament tether comprising 90 704 wire-to-wire bonds. The measured bonding yield of the manufacture was 99.9%. Wire-to-wire bond pull strength was measured in a separate test on a 97 m long tether produced subsequent to the 1 km tether production. The maximum sustainable pull force of the tether bonds should exceed the estimated 50 mN centrifugal force of the spinning full scale E-sail. The measured average maximum sustainable pull force of 252 bonds along the 97 m test tether was (99 ± 8) mN with a minimum recorded value of 80 mN.

This result shows that E-sail tether production on km scale is possible and thus supports the main claim of this thesis. Before this PhD project, no E-sail tether existed. The development of tether production and the results achieved brings the implementation of the most important E-sail component into the practical engineering realm and thus significantly advances the E-sail development. The produced 1 km tether was the most important objective of the ESAIL EU FP7 -framework project.

Publications

This thesis consists of a summary and two original core publications (I & II). The author of the thesis also made a significant contribution to six supporting publications (III–VIII). Publications are referred to in the text by Roman numerals (I–VIII).

I. H. Seppänen, S. Kiprich, R. Kurppa, P. Janhunen, & E. Hæggström, Wire-to-wire bonding of µm-diameter aluminum wires for the Electric Solar Wind Sail. *Microelectronic Engineering* **88,** 3267–3269 (2011).

II. H. Seppänen, T. Rauhala, S. Kiprich, J. Ukkonen, M. Simonsson, R. Kurppa, P. Janhunen, & E. Hæggström, One kilometer (1 km) electric solar wind sail tether produced automatically. *Review of Scientific Instruments* **84,** 095102 (2013).

III. I. Kassamakov, H. Seppänen, M. Oinonen, E. Hæggström, J. Österberg, J. Aaltonen, H. Saarikko, & Z. Radivojevic, Scanning white light interferometry in quality control of single-point tape automated bonding. *Microelectronic Engineering* **84,** 114–123 (2007).

IV. R. Schäfer, H. Seppänen, I. Kassamakov, E. Hæggström, & P. Hautpmann, Bonding quality monitoring applying statistical modeling of Scanning White Light Interferometry data. *Microelectronic Engineering* **84,** 2757–2768 (2007).

V. H. Seppänen, R. Schäfer, I. Kassamakov, P. Hauptmann, & E. Hæggström, Automated optical method for ultrasonic bond pull force estimation. *Microelectronic Engineering* **87,** 1796–1804 (2010).

VI. P. Janhunen, P.K. Toivanen, J. Polkko, S. Merikallio, P. Salminen, E. Haeggström, H. Seppänen, R. Kurppa, J. Ukkonen, S. Kiprich, G. Thornell, H. Kratz, L. Richter, O. Krömer, R. Rosta, M. Noorma, J. Envall, S. Lätt, G. Mengali, A.A. Quarta, H. Koivisto, O. Tarvainen, T. Kalvas, J. Kauppinen, A. Nuottajärvi, & A. Obraztsov, Electric solar wind sail: Toward test missions. *Rev. Sci. Instrum.* **81,** 111301 (2010).

VII. H. Seppänen, R. Kurppa, A. Meriläinen, & E. Hæggström, Real time contact resistance measurement to determine when microwelds start to form during ultrasonic wire bonding. *Microelectronic Engineering* **104,** 114–119 (2013).

VIII. A. Tietäväinen, T. Rauhala, H. Seppänen, R. Kurppa, A.I. Meriläinen, & E. Hæggström, Predicting bond failure after 1.5ms of bonding, an initial study. *Microelectron. Reliab.* **54,** 1452–1454 (2014).

Author's contribution

The author of this thesis contributed to the E-sail tether development by 1) manufacturing the first Hoytether-type E-sail tether sample (20 cm long) which demonstrated the manufacturability of E-sail tether. He also contributed by inventing 2) the wire-to-wire bonding technique, 3) the Heytether that eased 4-wire E-sail tether manufacturing without compromising micrometeoroid tolerance or tether mass, 4) the 3-wire wedge that enabled 4-wire Heytether production with a single wire bonder. As a lead engineer, the author 5) organized E-sail tether research, development, and manufacturing in 2006–2013. 6) The author planned the University of Helsinki (UH) work packages in ESAIL EU FP7 project, wrote the UH part of the application, and as a project manager executed the UH part of the project successfully.

The author's contribution to the publications:

I. The author invented the wire-to-wire bonding technique and the Heytether-type E-sail tether. The author planned and executed the measurements with the co-authors. The author wrote a major part of the paper.

II. The author invented the Heytether-type E-sail tether and 3-wire wedge and planned the experiment for producing the 1 km long E-sail tether. The author supervised the tetherfactory design and manufacturing as well as built and programmed the automatic quality inspection device of the tetherfactory. The author was one of the four main operators during the 1 km tether production. The author performed the data-analysis with author #5. The author wrote the paper.

III. The author manufactured tape automated bonds (TAB) for the experiment and performed pull tests. The author assisted in Scanning While Light Interferometry (SWLI) imaging, data analysis, and writing the paper.

IV. The author co-designed the experiment, manufactured TABs and performed pull tests. The author assisted in SWLI imaging and data analysis. The author wrote sections 1, 2, 5 and 6 of the paper.

V. The author co-designed the experiment, manufactured TABs and performed pull tests. The author assisted in SWLI imaging and co-analyzed the data. The author wrote sections 1, 2, 4 and 5 of the paper.

VI. The author invented the tether production techniques and supervised the tether manufacturing.

VII. The author invented and co-developed the real-time method for measuring the contact resistance development of the bond. The author supervised the measurements, analyzed data, and wrote the paper.

VIII. The author invented and co-developed the real-time method for measuring the contact resistance development of the bond. The author supervised the measurements and assisted in data analysis.

Acknowledgments

The work for this dissertation was done at the Electronics Research Laboratory, Department of Physics, University of Helsinki. I thank Prof. Hannu Koskinen and Prof. Juhani Keinonen for their support for the research.

I thank my supervisor Prof. Edward Hæggström for his support for the research, the knowledge he has shared and time he has spent advising and teaching me the world of science. I thank the inventor of the Electric Solar Wind Sail, Dr. Pekka Janhunen for his guidance during the tether production project. The tether production team Sergiy Kiprich, Risto Kurppa, Timo Rauhala, Jukka Ukkonen and Göran Macony made the major deliverable of this thesis. It still amazes me how well the team worked together to produce the 1-km long E-sail tether, that at one point was thought to be impossible or at least not practically possible. I thank Dr. Martin Simonsson for the support in research work and help in data-analysis and Dr. Greger Thornell for providing support in writing this thesis. I thank Dr. Anders Wallin, Dr. Ari Salmi and Kalle Hanhijärvi for providing valuable comments for this thesis.

I thank Dr. Markku Oinonen and Dr. Ivan Kassamakov for guidance for my first journal publications during my work in ALICE SSD project in CERN and Helsinki Institute of Physics. I also thank Detector Laboratory at the Helsinki Institute of Physics for supporting my research.

I thank my reviewers Prof. Michael Mayer and Dr. Robert Hoyt for their efforts to review this thesis and Prof. Jörg Wallascheck for accepting the invitation to be an opponent in the defense of this dissertation.

I am grateful for the Väisälä foundation, Vihuri foundation, Magnus Ehrnrooth foundation, the Chancellor of the University of Helsinki and EU FP-7 program for financial support for my research.

Finally, I thank my wife Selma, for her support and patience during the work.

Henri Seppänen

Contents

1. Introduction

The Electric solar wind sail (E-sail) is a space propulsion device for interplanetary missions [1]. In this chapter, I give a brief introduction to solar system exploration followed by an introduction to the E-sail concept, and to ultrasonic wire bonding—the method of choice for E-sail tether manufacture.

1.1. Solar system exploration

Solar system exploration started in 1957 by the first Earth orbiter, Sputnik 1. Since then more than 180 spacecraft have been launched to explore and expand our understanding of the solar system [2]. New knowledge has been gathered to elucidate the formation of the Sun, planets, moons, asteroids, and other solar orbiters [3, 4]. This knowledge has improved our understanding of the present state of the Earth and may in the future help preserve our home planet.

New information about the solar system has primarily been gathered by interplanetary missions [5]. An interplanetary mission transfer usually requires large changes in orbital energy, which in a conventional (chemical) propulsion system requires considerable propellant mass [6]. An option to reduce the propellant mass and mission costs is generated by combining a chemical thruster with a low thrust propulsion system, such as the E-sail [3, 6].

1.2. Electric solar wind sail

The E-sail (Fig. 1) uses long, thin, centrifugally stretched and positively charged tethers to create thrust from the momentum flux of the solar wind [1]. This propellant-less device is free from the limitations set by the rocket equation and therefore holds promise for scientific exploration and commercial use of our solar system [VI, 7, 8].

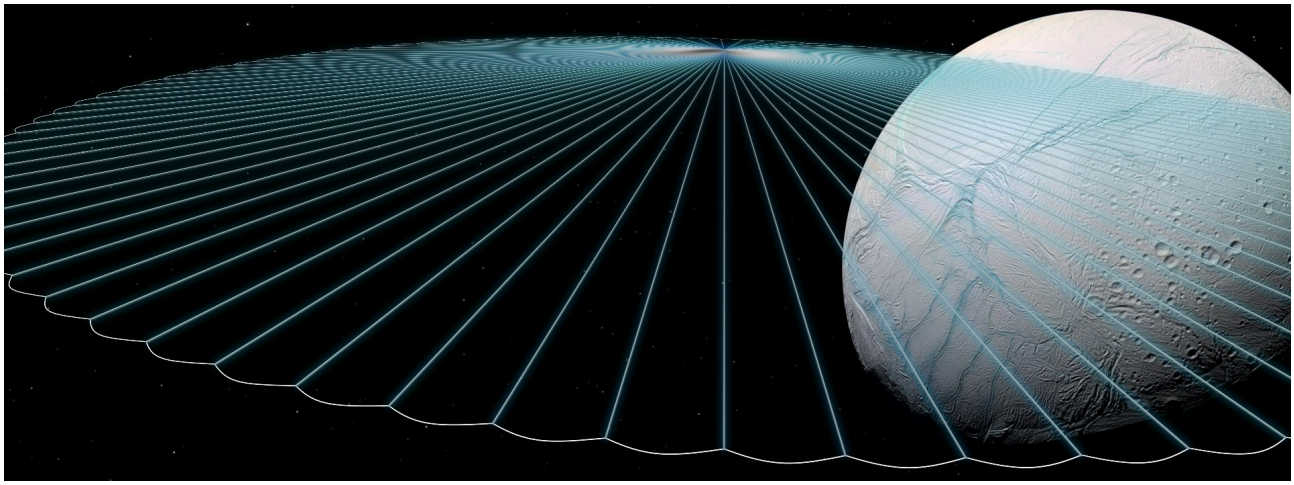

Figure 1. Conceptual figure of the E-sail. Each centrifugally stretched tether is 20 km long. Tethers are stabilized from the tip by auxiliary tethers. The solar wind pressure makes the charged E-sail cone shaped. The estimated transfer time to Saturn is 4 years [6]. (Background image: Saturn's moon Enceladus, NASA/JPL/Space Science Institute).

1.2.1. E-sail force

A thin conducting wire that is kept at positive potential with respect to the solar wind plasma features an electric field around itself [I]. Incoming solar wind protons interact with the electric field and part of the proton momentum is transferred to the wire [VI]. This physical phenomenon, plasma coulomb interaction, creates the E-sail force. It has not been measured experimentally yet, but indirect estimation, based on laboratory measurements by Siguier *et al.* [9], has been made [10].

A charged tether immersed in moving plasma receives thrust F (the E-sail force). An estimate of the thrust per unit length is

$$\frac{dF}{dz} \approx 0.18\, V_{tether} \sqrt{\epsilon_0 P_{dyn}}, \tag{1}$$

where V_{tether} is the tether voltage, ϵ_0 is vacuum permittivity, and P_{dyn} is the dynamic pressure in the solar wind [VI]. A tether charged to 20 kV in average solar wind conditions produces 500 nN/m thrust at 1 AU (astronomical unit) [VI, 11], which means that an E-sail composed of 100 tethers, each 20 km long, would provide 1 N thrust [VI, 11].

1.2.2. Tether requirements

The E-sail tethers are centrifugally stretched. The centrifugal force must overcome the expected solar wind force by a factor of five [VI]. The tethers should mechanically withstand the centrifugal force of the spinning E-sail. For a 1 N E-sail the solar wind force per tether is 10 mN which means that in normal operating conditions 50 mN centrifugal force is present [VI]. This sets the minimum required pull strength of the tether to 50 mN.

The tethers are kept positively charged by an onboard electron gun [1]. However, in space positively charged tethers collect electrons that neutralize its charge. To transfer electrons to the electron gun, the tethers need to be conductive. In practice, steel provides sufficient conductivity (7×10^6 S/m) for E-sail tethers [12], whereas the conductivity of aluminum bonding wire is five times higher than that of steel. Another, related requirement is that the electron collecting surface of the tether should be small to minimize the power necessary to keep it charged [13]. In general, a round cross section minimizes the surface area in a thin rod.

The E-sail tether should feature micrometeoroid tolerance. An interplanetary E-sail mission can last from half a year to 14 years [6]. During that time, the E-sail tethers are exposed to (micro)meteoroid impacts that may cut the tether. Micrometeoroids are particles of natural origin in space whose mass is less than one gram. Meteoroid flux, f, is defined as the number of intercepted objects per area per unit time [14]. In practice, meteoroid flux is the cumulative flux of particles larger than a specified diameter [15]. For thin wires, f is converted to lethal impactors (f_k) by assuming that the wire may be cut by micrometeoroids smaller than the wire diameter [15]. In ref. [15] it was assumed that meteoroids exceeding 0.3 times the wire diameter may cut the wire. The rate of cuts of a single round wire is calculated from the lethal micrometeoroid flux multiplied by the wire surface area A

$$c = A\, f_k = \pi d l\, f_k, \tag{2}$$

where d is wire diameter and l is wire length [15]. The number of single wire cuts during the time t is $n = c\ t$ whereas the survival probability of a single wire is

$$S(t) = e^{-c\,t}. \tag{3}$$

The Hoytether is a multifilament net consisting of a number of primary wires cross-linked by diagonal secondary wires [16]. A Hoytether features h segments or levels determined by the interconnection points between primary lines and secondary lines (Fig. 2). Based on [15] the probability of survival of the Hoytether is the product of the survival of all h primary line levels in the tether as a function of time (t):

$$S(t) = \left(1-\left(1-e^{-c_p t}\right)^x \left(1-e^{-c_s t}\right)^y\right)^h, \tag{4}$$

where c_p and c_s are the rate of cuts of the primary and secondary wires in the single level and x and y are the number of primary and secondary wires. Equation (4) shows that making primary line levels shorter, while keeping the tether length constant (reducing c_p and c_s) and/or increasing the number of primary and secondary wires significantly improves the survival probability of the Hoytether. This important finding for the space tether design made the Hoytether the initial option for the E-sail tether [VI].

The redundancy that the multifilament structure creates makes the tether robust against both micrometeoroids in space and bond failures during production. The required tether bonding yield in the ESAIL EU project was 99%, a number that was considered sufficient for the required micrometeoroid survival probability.

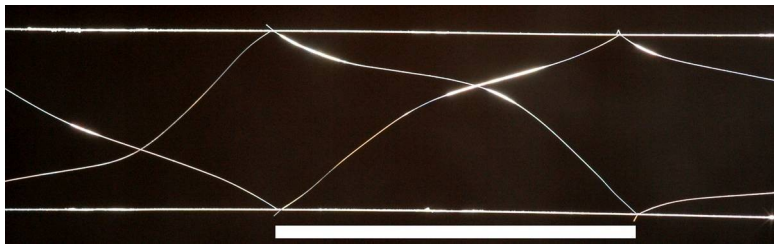

Figure 2. Four-wire Hoytether structure [VI]. The diagonal secondary wires (Al, Ø = 25 μm) are ultrasonically bonded to the horizontal primary wires (Al, Ø = 75 μm). The white bar is 23 mm long and indicates one primary line level. In this Hoytether $x = y = 2$.

1.3. Ultrasonic bonding

Wire bonds have been used in billions of electronic devices since the 1947 when the interconnecting technique was invented [17]. Wire bonding is typically an electromechanical connection between a bonding wire and a pad [17]. One form of wire bonding, ultrasonic bonding uses ultrasound energy to clean the bonded surfaces and mechanical pressure to make the surfaces bond by adhesion [17, 18]. The most common use of ultrasonic bonding is to connect microchips electrically to their packages by thin (Ø = 25–50 μm) aluminum wires [17]. Ultrasonic bonding is not thermally activated and is typically done at room temperature [18, 19].

1.3.1. The ultrasonic bonding process

Ultrasonic bonding takes place via a sliding friction process [20]. However, the theory of the bonding mechanism is not fully understood [21, 22]. During the ultrasonic bonding process a wire is pressed against the pad by a normal bond force, ca 0.2–1 N for 10–50 ms. The process starts when a sinusoidal electric signal is applied to an electromechanical piezo element. This element generates a longitudinal ultrasonic motion into an acoustic horn that translates vibrations to the wedge (Fig. 3). The ultrasonic bonding process is divided into four phases [20]:

1) Initially during the *stiction phase* the ultrasonic vibration force is weak and does not overcome the static friction between the wire and the pad [22]. In this phase, the bonding interface does not develop [22]. The duration of this phase is 2 to 3 ms [20, 22, 23]. In ref [VII] the first changes in bond interface resistance were measured at 1 ms into the ultrasonic process. These changes indicate that microslipping takes place at the bond interface before break-off occurs [24].

2) Phase 2, *the cleaning phase*, starts with a break-off when the relative displacement between the wire and the pad starts [20]. After break-off the wire and pad interface start to clean by wear but no bonding occurs yet [VII, 20]. The duration of the second phase is ca 1.5 ms [20].

3) During phase 3, *the welding phase*, the adhesion between the cleaned surfaces increases the friction and the first microwelds appear [20]. The welding process continues and the bonded area increases [VII, 22]. The duration of Phase 3 is typically 10 to 20 ms [20].

4) It is assumed that the microwelds do not grow in phase 4, *the diffusion phase* [20]. However, the wire deformation continues as long as ultrasonic energy is applied to the bonding. This deformation may weaken the neck of the bond [22].

The bonding process is sensitive to the bonding parameters (ultrasonic time, ultrasonic power, bond force), bonded materials, surface cleanness, and wedge attachment to the horn. For example too high a bond force may lead to poor cleaning during phase 2 and a too extensive wire deformation in phase 4. However, by optimizing the bonding process it is possible to ensure high yield and high quality bonds that are essential for the ultrasonically manufactured space tethers.

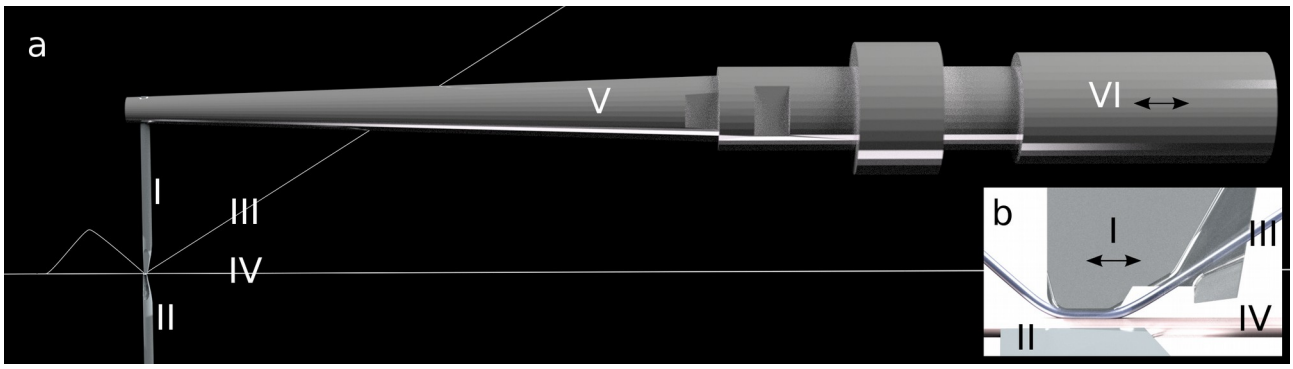

Figure 3. Schematic figure. (a) Core elements of the ultrasonic bonding device and (b) cross section of the bonding spot. (I) Bonding wedge, (II) base wedge, (III) loop wire, (IV) base wire, (V) horn, and (VI) piezo. The piezo element generates longitudinal vibration that translates and is amplified through the horn to the wedge (arrows). The wedge presses the loop wire against the base wedge and forms the wire-to-wire bond.

1.3.2. Wire bond quality

The ultrasonic bond interface and neck affect the bond quality most (Fig. 4). The neck may be over-deformed by a too long bonding time, a too high bond force, and/or too high ultrasonic power. An over-deformed neck is significantly weaker than the bond interface. On the other hand, the bond interface may remain weak if the bonding process ends too early or if the ultrasonic power—bond force combination is poorly optimized.

The ultrasonic bonds are the weakest part of the E-sail tethers. Therefore the bond quality needs to be tested to qualify the tether.

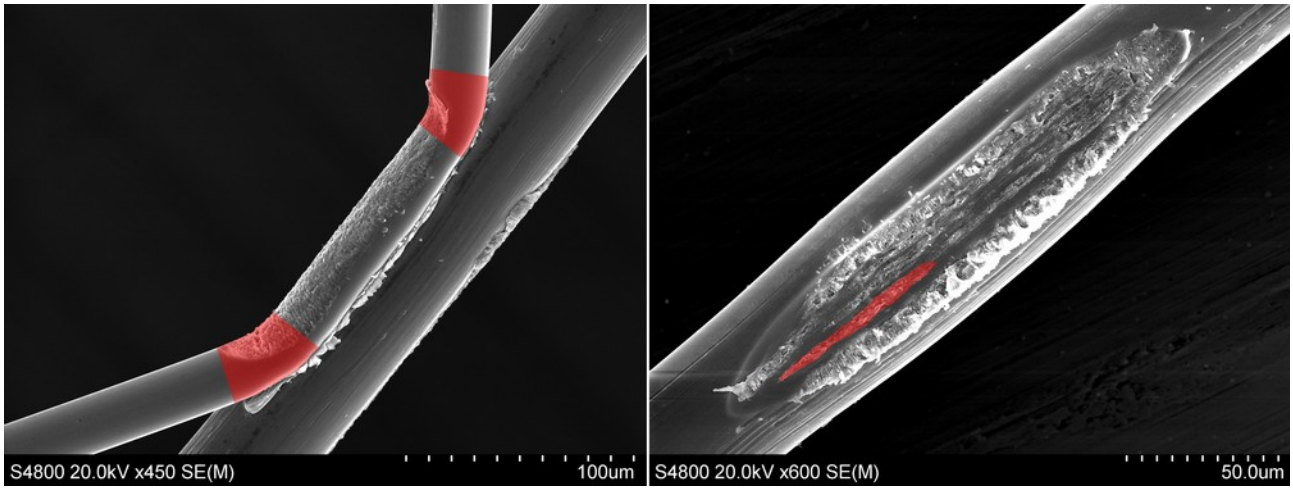

Figure 4. SEM images of an ultrasonic wire-to-wire bond and a bond interface after the wire is lifted. Red highlights on the left image indicate the two necks of the bond. The shape of the neck affects the mechanical strength of the bond. In the right image one of many microwelds is highlighted. The sum of all microwelds is the bonded area that provides mechanical strength and electrical conductivity.

The gold standard to test ultrasonic bond quality is the destructive pull test [25]. It measures the maximum sustainable pull force of the bond by breaking it at its weakest point, either the interface

(lift off) or neck (cut off). Typically, destructive pull tests used to qualify bonds allow testing only a fraction of the bonds [26]. The rest of the bonds are assumed to follow the statistical distribution of the test. However, drifts in the process as well as discrete effects such as bond pad contamination, tool wear or other unpredictable reasons can lead to weak bonds [27]. In production where high reliability and quality are needed (e.g. essential electronics of complex and expensive facilities), one must therefore test each bond [28].

1.3.3. Bonding process control

Real-time process control is used in modern automatic wire bonders [29]. Typically such process control measures wedge displacement along the horizontal and/or vertical direction directly or indirectly. For example, information about wire deformation and/or the mechanical impedance seen by the wedge are used to control in real time the bonding parameters (ultrasound power, bond force, bonding time)[30], [31].

One option for online process control is an optical Non-destructive Test (NDT) method that provides information about the bond strength by comparing the bond geometry to predefined model values (soft modeling, and look-up tables) [32], [33]. Regions of interest (ROI) in the bond geometry image are typically pre-selected by the operator [III], [33]. The optical method can be used when the bond is visually accessible.

1.4. Aims and scope of the research

The aim of this thesis is to prove that km long E-sail tether production is possible.

Paper [I] and [II] ask whether a full scale E-sail tether can be produced. Can tether production be automated and is it scalable? Can quality be assured? What is the quality of the tether after production and what are the causes of the failures? What is the maximum sustainable pull strength of the tether during production? A tether factory that produces multifilament tether is presented and the results of the production are shown. An online optical method to measure bonding success is used to estimate the final quality of the produced tether. An offline destructive pull test was used to determine the maximum sustainable pull force of the bonds in the test tether.

2. Methods and measurements

This chapter introduces methods for E-sail tether manufacturing and quality control.

2.1. Wire-to-wire bonding

Wire-to-wire bonding is a method to ultrasonically bond two metal wires together. The method was developed specifically for the E-sail tether production. The process to produce wire-to-wire bonds was first presented in paper [I], whereas in paper [II] the wire-to-wire bonding technique was used for tether production. Wire-to-wire bonding is performed on wires running parallel to each other. In the process, the loop wire is ultrasonically bonded to the base wire. To provide a stable base for bonding, the base wire is fixed by the base wedge and two clamps whereas the loop wire and loop formation is controlled by the bonder.

2.1.1. Wires

The bond pad and the wire are equally hard in classical wire bonding [17]. We chose a Ø = 50 μm medium hardness wire Al(1%Si) as base wire onto which a Ø = 25 μm soft wire Al(1%Si) was bonded. A large base wire makes the bonding process easier relatively speaking by providing a wide bonding spot. This wire combination fulfills the E-sail requirements with regards to wire strength, outer surface area [10], and availability for large scale production. The 50 μm wire features a breaking load of 600–660 mN whereas the 25 μm wire has a 130–150 mN breaking load.

2.1.2. Wedges

A custom made base wedge was designed to provide, with minimum base wire deformation, a firm support for the base wire and to allow easy bond removal after completing the wire-to-wire bonding process. The key requirement in the base wedge design was to restrict the wire displacement during the ultrasonic bonding process.

In paper [II], a custom designed 3-wire wedge was used to bond three loop wires onto one base wire with a single bonder (Fig. 5 & 6 b, d). A special design included grooves along the wires, large polished front and back radii, and tall openings for wire guides. This design was chosen to improve the neck shape and strength as well as to reduce the bending of the bond neck and dynamic friction when the wire was translated inside the wedge.

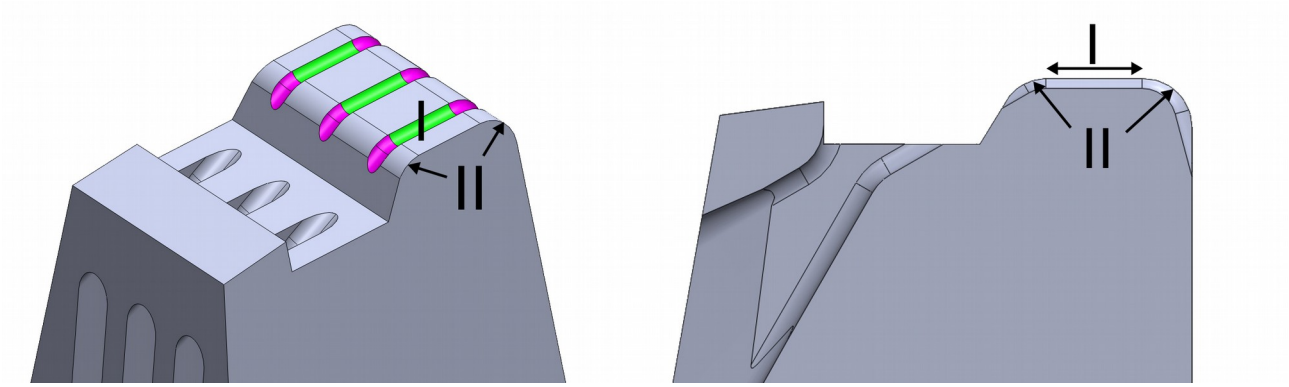

Figure 5. Schematic figure of the tip of the 3-wire wedge. A 100 µm long grooved foot (I) (green) and large 50 µm forward and backward radii (II) (purple) were designed to ensure bonds with high pull strength by minimizing wire neck deformation.

2.1.3. Flattening

Since existing bonding equipment and tools are designed for bonding to flat pads, the base wire should present a flat surface in the bonding area. The base wire was therefore flattened by indenting it with a metal cylinder after positioning the wire in the groove.

2.1.4. Wire alignment

Grooves in the 3-wire wedge improve the wire position accuracy during bonding. This is important since the bonding spot on the base wire is only approximately 5 µm wide. The grooves also improve the neck shape while limiting neck deformation, as well as keep the neck shape round.

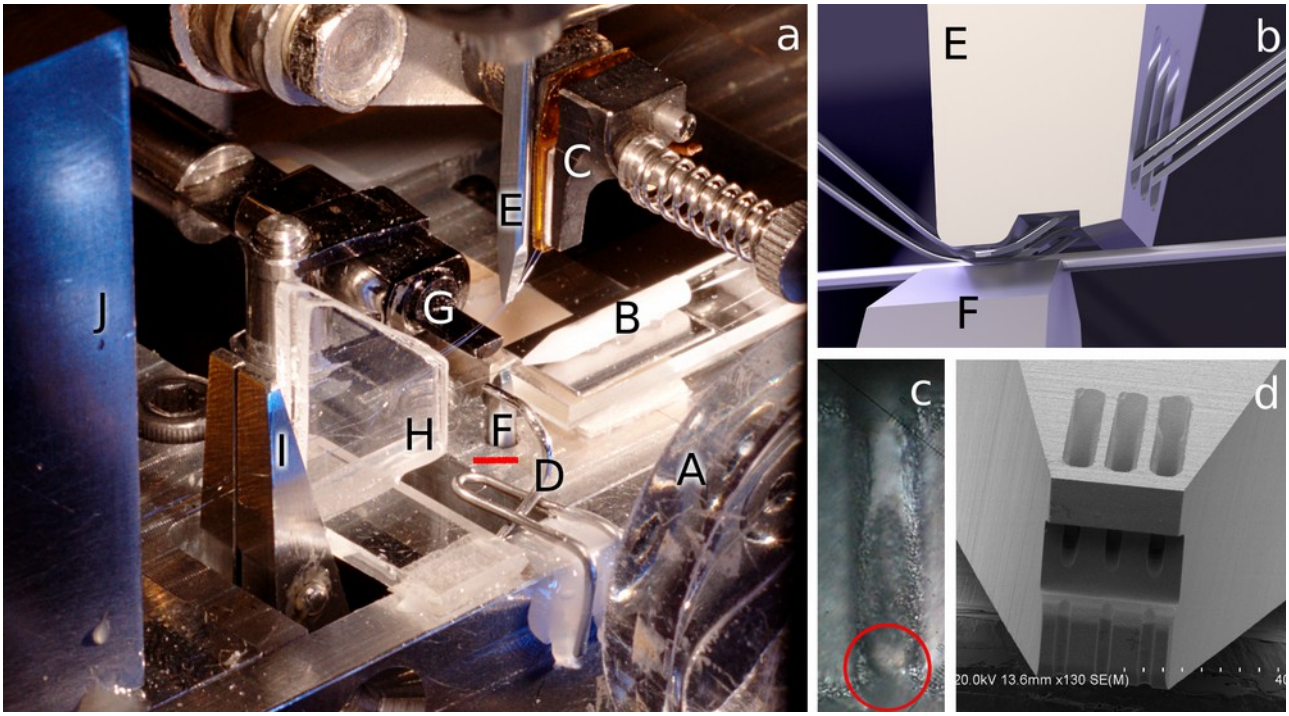

Figure 6. (a) Tether bonding. (A) Microscope camera, (B) capillary guide for base wire, (C) clamp guide for loop wires, (D) pin for creating loops, (E) 3-wire wedge, (F) base wedge, (G) flattening tool, (H) glass guide, (I) second clamp, and (J) wire guide. The red bar below F is 2 mm long. (b) Simulated image of 3-wire wedge during bonding and (c) microscope image of one contaminated groove of the 3-wire wedge. Aluminum accrues in the groove and reduces the neck width (red circle). (d) SEM image of 3-wire wedge. A multimedia presentation of the wire-to-wire bonding and tether manufacturing is included in the online files of paper [II].

2.2. Tether production

2.2.1. Heytether

The Heytether is a tether structure featuring a single straight base wire onto which multiple loop wires are bonded. The Heytether was designed to maximize the micrometeoroid resistance by means of a multifilament structure and to minimize the tether mass and surface area by allowing thin round wires to be used in the tether. The Heytether structure permits tether production on large scale since it employs a relatively simple single base wire design to which multiple loop wires are bonded. A 4-wire Heytether section is illustrated in Fig. 7(I).

The base wire of the intact Heytether carries the full centrifugal load caused by the spinning E-sail. However, micrometeoroids cut the 20 km long base wire (Ø = 50 μm) at an estimated rate of 160 cuts/year (f_k = 52/m^2/year [14]). At the site where the base wire is cut the shortest intact loop wire comes under load. Simultaneously the other intact loop wires remain separated to minimize the probability that a single meteoroid cuts the entire tether (Fig. 7(II)). Based on Eq. (4) the survival probability as a function of time of the Heytether is

$$S(t) = \left(1-\left(1-e^{-c_b t}\right)\left(1-e^{-c_1 t}\right)\left(1-e^{-c_2 t}\right)\left(1-e^{-c_3 t}\right)\right)^h, \tag{5}$$

where c_b, c_1, c_2, c_3 are the rate of cuts to the single level base and loop wires (Eq. (2)). For a Heytether as described in table 1 the survival probability in a 5 year mission is 99.9994%.

Table 1. Heytether parameters

Parameter	Value	Parameter	Value
Loop length *(l)*	30 mm	Tether length *(tl)*	20 km
Loop wire heights	5, 10, 15 mm	Number of loops = levels *(h = tl/l)*	667 k
Loop wire lengths	34, 43, 56 mm	Mission time *(t)*	5 years
Base wire diameter	50 μm	Micrometeoroid flux (size > 16 μm)[14]	52 m^{-2} $year^{-1}$
Loop wire diameters	25 μm	Micrometeoroid flux (size > 8 μm)[14]	112 m^{-2} $year^{-1}$

The survival probabilities for the Heytether and a comparable Hoytether structure are similar. Equation (5) takes into account micrometeoroid hits where only one wire is cut at the time whereas larger meteoroids may cut the entire tether in one hit. The probability that a meteoroid larger than 1 cm hits the tether during a 5 year mission is 0.03% whereas it is 0.5% for meteoroids larger than 0.5 cm [14].

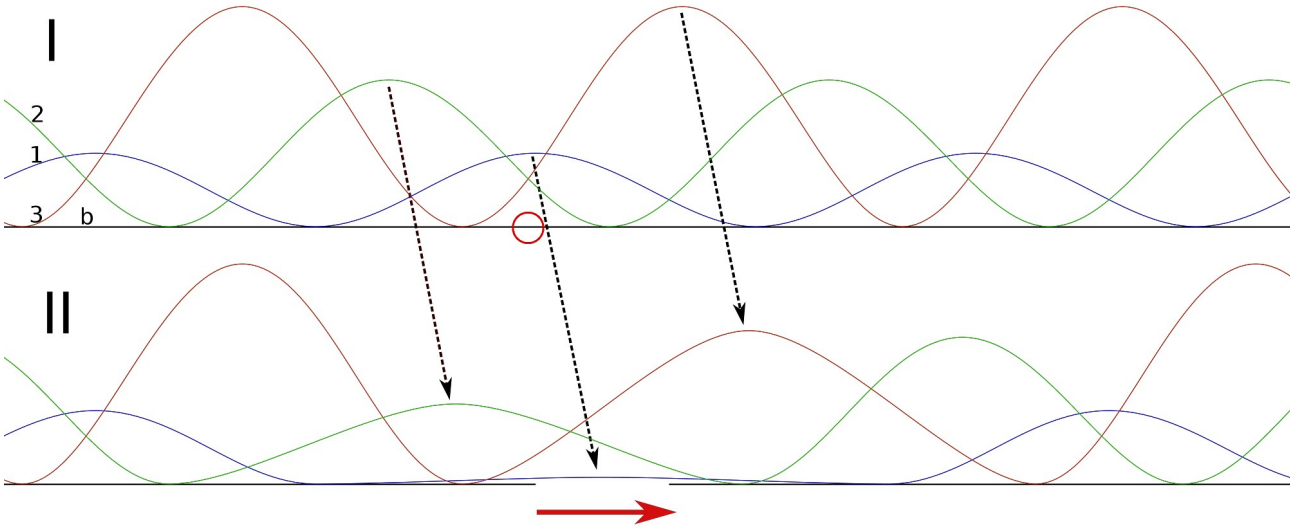

Figure 7. Schematic figure of intact Heytether (I) and Heytether after a base cut (II). 4-wire Heytether is made of three loop wires (1,2,3) and single base wire (b). Red circle marks the site of the cut. The centrifugal force pulls the base wire in the direction marked by the red arrow. Loop wire deformations after the cut are illustrated (dashed arrows). Ideally loop planes and lengths differ to reduce the possibility that a single micrometeoroid cuts all wires.

2.2.2. Tetherfactory

For km scale tether production we constructed an automated tetherfactory (ATF) with a machine-vision based quality assurance system. The ATF is built around a customized manual bonder (Kulicke & Soffa 4123) and a tether factory (Fig. 8). During tether production, all operations were controlled by two computers and three microcontrollers (Arduino). The tether production cycle is visualized in Fig. 10 and

the timeline of one cycle is seen in Fig. 16a. Some highlights of the tetherfactory development are shown in Appendix A.

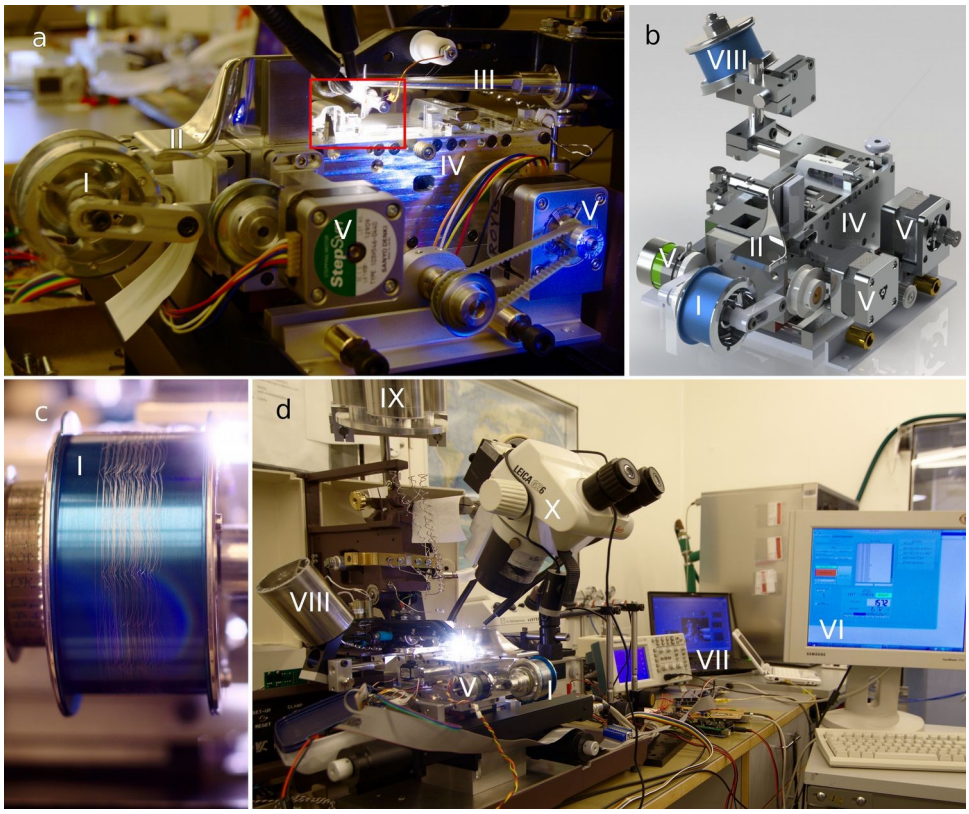

Figure 8. (a) Photograph of the automatic tetherfactory that bonds three loop wires onto one base wire to form a 4-wire tether. (b) Schematic figure of the tetherfactory. (c) The 4-wire tether reeled onto a spool at the beginning of the tether production. (d) The tetherfactory integrated with a customized wire bonder and controlled by the computers and multiple microcontrollers. In automatic mode 70 m of tether is produced in 24 hours (11 sec per bond). Marked in the images: (I) Spool, (II) wire guide, (III) horn, (IV) base, (V) motors, (VI) controlling computer, (VII) quality inspection computer, (VIII) base wire input spool, (IX) loop wire input spools, (X) optical microscope for visual inspection. Red square indicates the location of the Figure 6(a) view.

2.3. Tether quality

2.3.1. Destructive pull test

The destructive pull test is a method to estimate the absolute value and the statistical variance of the tether pull strength at its weakest points, the wire-to-wire bonds. The minimum required pull strength is 50 mN. In our device, a base wire was attached at its ends to a jig, cut in the middle under the loop and then pulled along the wire direction. The maximum sustainable pull force was measured with an electric scale. This test simulates the force that stresses the wire-to-wire bonds during space flight after a micrometeoroid has cut the base wire (Fig. 7(II)). The test is different from the traditional destructive pull test where the wire is pulled perpendicular to the bond pad [25]. Even though the destructive pull test estimates the quality of

the attached bonds, we also measured the rate of the wire-to-wire bonds that failed to attach during production by an inline tether quality assurance method.

2.3.2. Tether quality assurance

The core of the quality assurance system is a microscope camera (Veho VMS-004D) and a custom-made NI LabVIEW based image acquisition software that analyzes a binarized camera image of the region of interest (ROI) (Fig. 9). The image analysis assures that (1) the wedge contact takes place at the correct instant of the bonding cycle (marked 'bonding' in the online video accompanying paper [II]), and (2) the loop wire remains in contact with the base wire after the wedge is retracted. This approach allows verifying that the loop wire adheres to the base. In cases where this does not happen a new bond is made next to the failed one. During each wedge retraction, an image was taken, analyzed, and saved. Similarly, each operation carried out by the master Arduino (microcontroller) was stored in a log file. The log file was later used to categorize tether production failures. In addition, the operator actions such as wedge cleaning, putting the base wire back into the base wedge groove, and restarting the bonder after electronics failures were recorded by hand.

The tether quality assurance system was built to indicate the rate of failed bonds during the production and to halt the automatic production if two consecutive bonds failed. The actual category of failure was determined during post production analysis.

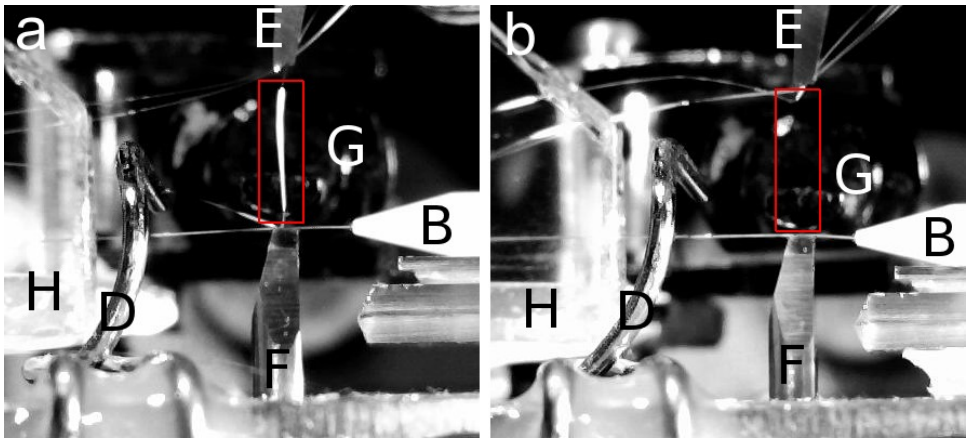

Figure 9. Two images obtained by the quality assurance microscope camera. “Good” (a) and “failed” (b) bond. The red square indicates the ROI area inside which the bonding wire was searched for after the bonding process. The indicator letters correspond to those in Fig. 6.

2.3.3. Post production analysis

Post production analysis to determine the failure rate and -types was done based on the stored images as well as on the computer and handwritten logs. CellProfiler [34] and R software [35] permitted handling large amounts of data during automated image analysis and data processing. ImageJ software [36] was used to manually find and delineate the ROI of the expected wire location between the two edges (see Fig. 9). The mean intensity in the ROI was measured in all images in each batch. The batch was a set of images taken between manual interventions necessary to move the microscope camera of the factory. If the measured intensity in an image deviated by more than 4.5 sigma from the mean of the batch, the image

was manually analyzed and compared with the logs. During manual image analysis an operator visually defined whether the bond was 'good' or lifted ('failed'), whereas the handwritten and computer generated logs helped to define repaired (initially 'failed') bond category and the cause of the failure. All stored images were analyzed by computer and 401 images were analyzed by hand.

A bond was considered “good” if it remained bonded after the wedge was retracted, whereas it was considered “failed” if it either (1) remained lifted also after a rebonding attempt or (2) the wire was cut. A “repaired” bond is a bond that was initially lifted, but later successfully rebonded next to the original spot.

Figure 10. Flow chart of tether production cycle. The cycle is visualized in a multimedia presentation included in the online files of paper II.

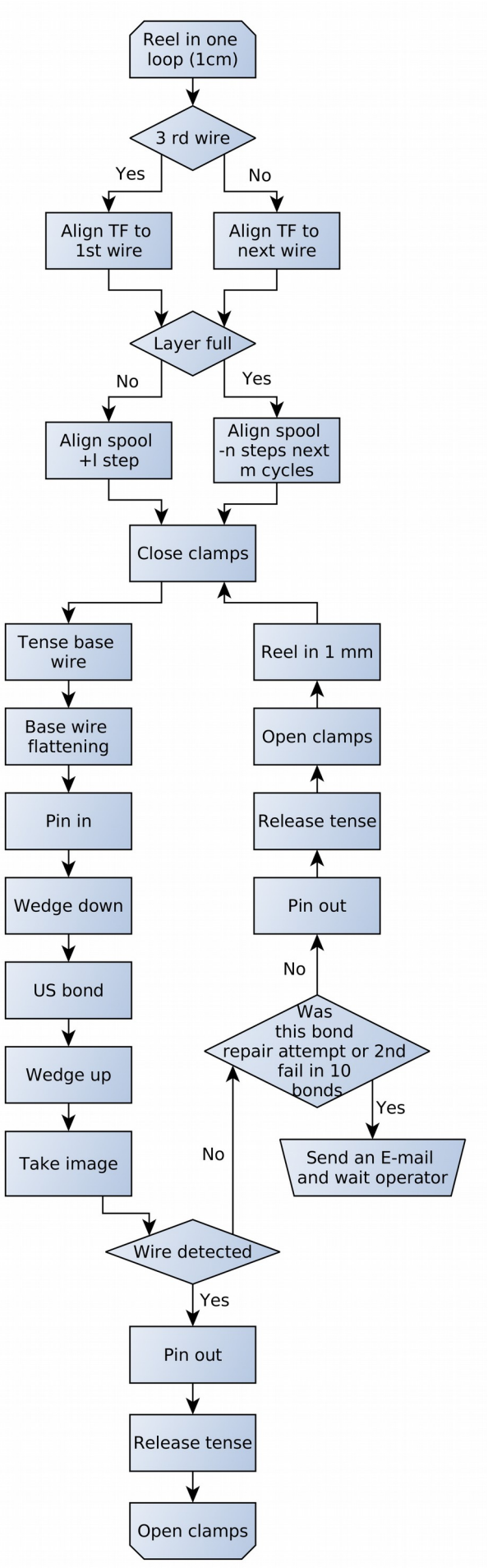

3. Results

3.1. 1 km tether

The wire-to-wire bonding technique was used to produce a 1.04 kilometer long multifilament 4-wire tether comprising 90 704 wire-to-wire bonds. The results were published in paper [II]. The multifilament tether features a Ø = 50 µm Al base wire onto which three Ø = 25 µm loop wires were bonded (Fig. 11). The production rate was 70 m / 24 h (11 s / bond) and a quality level of 0.1% failed (loose) bonds and 0.2% repaired (rebonded) bonds was reached.

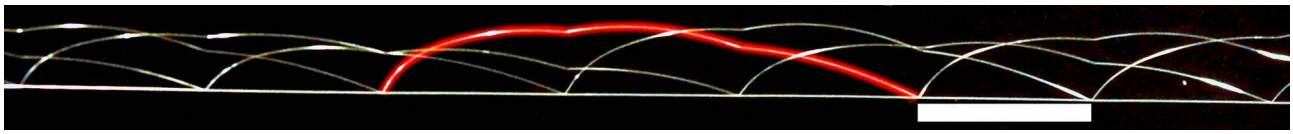

Figure 11. Multifilament 4-wire tether produced right after the 1 km tether production. The red highlight shows one full loop. The white bar is 10 mm long.

The average distance between bonds on the base wire was 11.5 mm starting from 10 mm at the beginning of the production and reaching 13 mm at the end of the production. The increase was due to accumulating tether layers on the output reel. Figure 12 shows the final 1.04 km long tether.

Figure 12. The manufactured 1.04 km long 4-wire tether on a production reel. The weight of the tether is 11 g.

3.2. 1 km tether quality

Table 2 lists the production statistics as determined from the production log and image analysis. 82 bonds out of 90 704 bonds remained failed after the bonding process. That is 0.1% of the produced bonds. 74 of 82 failed bonds remained lifted and 8 times the loop wire was cut. 192 times the loop wire was first lifted, but repaired automatically. The base wire was cut three times and repaired. Twice the base wire broke during the production because the base wire was stuck inside the spool and once the base wire was cut intentionally to replace a broken clamp control servo. The base wire was repaired in a seven steps. 1) The 3-wire wedge was changed to the single bond wedge designed to bond 50 µm wire. 2) The broken base wire was carefully pulled back and fed from the bottom (foot) into the wedge. 3) The original base wire was adjusted between the clamps to the normal bonding spot on top of the base wedge and flattened. 4) The

two base wires were bonded together. Two or more bonds were performed in a row. 5) The 3-wire wedge inserted into the bonder and 6) the new continuous base wire was pulled back into the position that enables 7) loops to be bonded across the repaired base wire joint.

Table 2. 1 km tether production quality statistics

Failure mode	Repaired bonds	Repaired base wire	Failed bonds	Loop wire cut	
Bond lifted	173	...	47	...	
Base wire out of groove	1	...	17	...	
Wires stuck	2	...	3	1	
Bad alignment	...	...	3	1	
Control electronic failure	6	1	1	...	
Other	10	2	3	6	
Total (sum)	192	3	74	8	Σ 277 (0.3%)
	Σ 195 (0.2%)		Σ 82 (0.1%)		

The cumulative plot in Fig. 13 shows failed and repaired bonds during 1 km tether production. Compared to the overall 0.1% failure rate, between 5000 and 65 000 produced bonds the failure rate was 0.05% (31 failures/60 000 bonds) whereas the failure rate in the 5000 bonds produced right after wedge cleaning was 0.06%. The number of failures around 70 000 produced bonds was caused by a problem in a clamp control servo.

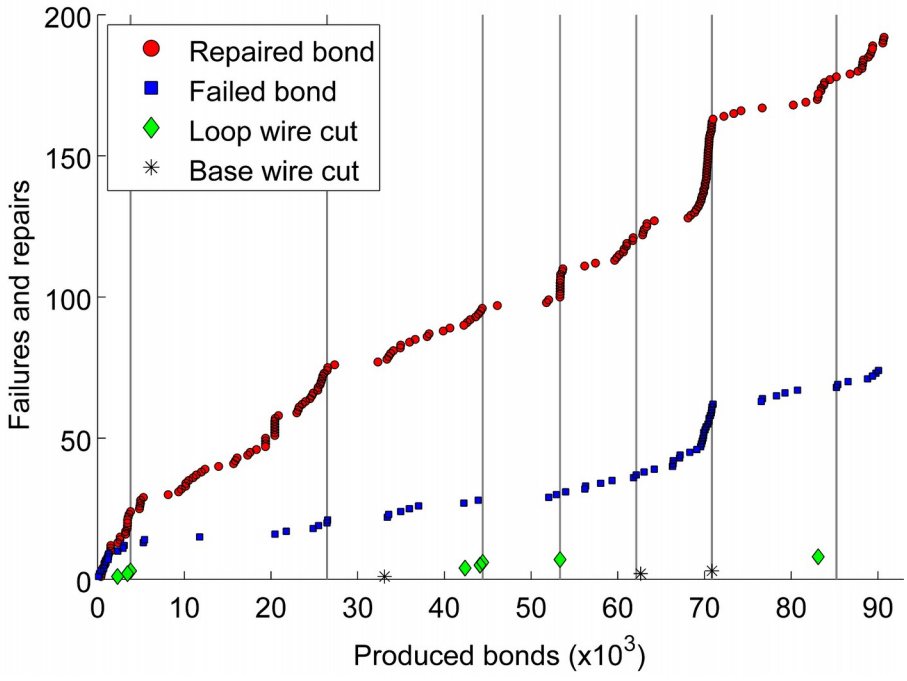

Figure 13. Failures and repaired bonds during manufacturing as determined from the production log and image analysis. 0.1% of produced bonds remained lifted (failed) and 8 times the loop wire was cut. Wedge cleanings are marked by vertical lines.

Destructively measured maximum sustainable pull force of 252 bonds are shown in Fig. 14. These bonds were measured along a 97 m long tether produced right after the 1 km tether production (post

production). The measured average maximum sustainable pull force was (99 ± 8) mN whereas the minimum value was 80 mN.

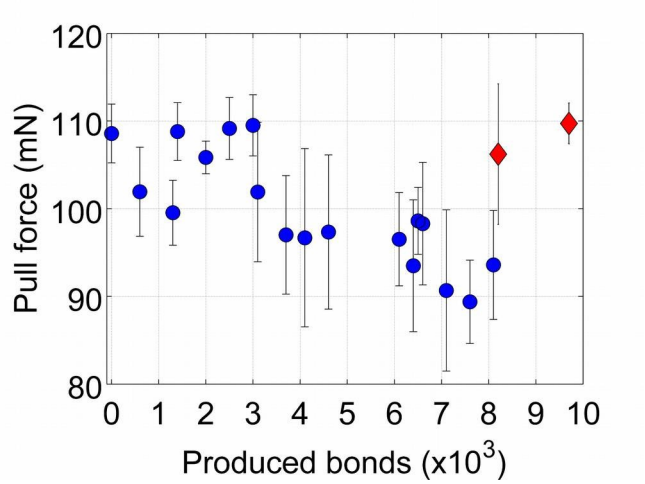

Figure 14. Measured maximum sustainable pull force along the 97 m post production tether. Each point comprises 6–16 measurements and the error bars indicate one standard deviation. Altogether 252 bonds were measured. The measured average maximum sustainable pull force was 99 ± 8 mN and the lowest measured value was 80 mN. The two last measurements, marked as red, were done after wedge cleaning.

4. Discussion

The aim of this thesis is to show that E-sail tethers can be manufactured on km scale. Here I discuss the validity of the achieved results and their implications.

4.1. E-sail tether manufacture on km scale

In paper [I], the capability to bond two Al wires together—wire-to-wire bond—was shown for the first time. Wire-to-wire bonding, the core building block of the E-sail tether, was used to produce a 1 km long 4-wire multifilament tether (paper [II]). This result shows that manufacturing multifilament E-sail tether on km scale is possible.

4.1.1. Impact on the field of solar system exploration

The 1 km long tether was a milestone in the E-sail development. The tether development project at the Electronics Research Laboratory (ERL, Department of Physics, University of Helsinki) began in 2007 from a need stated by the E-sail community that previously only had carried out simulation work [13], [37]. At that time, no tether for the E-sail existed. Since then the technology readiness level (TRL) of the tether has reached TRL 4-5 [10], [38]. E-sail tether development continues in co-operation with the ERL and the Finnish Meteorological Institute. In addition to the previous major funding bodies (EU and the Academy of Finland), recently NASA (National Space Agency, USA) has shown interest to fund the project [39].

Interest to use the tether for satellite deorbiting has increased after the successful ESAIL EU -project [40]. In such an experiment, a tether is used as a low mass and low cost plasma brake after the lifetime of the satellite has been reached [41].

In the ESTCube-1 satellite, a short (< 10 m) two-wire tether was launched into a LEO orbit [42]. The goal of that mission among other things is to measure, for the first time, the magnitude of the E-sail force (plasma coulomb interaction) in space. Similar experiments are planned for the Finnish AALTO-1 and -2 satellites [43].

4.1.2. Impact on the microelectronic wire bonding field

The tether production is an esoteric example in the field of microelectronic wire bonding. The achievement shows the versatility of the interconnection technique. The versatility of the wire bonding technique has kept it the number one interconnection technique for more than five decades [17]. Due to its nontraditional nature, the impact of the tether production on the microelectronic wire bonding field itself may be low. However, the tether production project could not have been successful without the deep knowledge gathered before and during the project. The final impact of this knowledge (9 published journal papers and 12 conference papers) is still to be seen [I–VIII], [24], [44–55].

4.2. Discussion of results

4.2.1. Wire-to-wire bond quality

The ultrasonic process parameters are optimized to create maximum performance in selected test(s). The wire-to-wire bonds were primarily optimized to maximize pull force in a pull test that simulates the centrifugal pull in space after micrometeoroids have cut the base wire (see Fig. 7). The secondary test criterion was to minimize bond failures during tether production.

The primary criterion produced a wedge design that minimizes bond neck deformation while being able to weld a large interface area. This was achieved by a wedge that featured a long foot (100 μm), a groove along the wire, and large front and back radii (50 μm) (Fig. 5). The process parameters were selected to produce 20% wire deformation (the wedge penetrates into the wire 0.2 times the wire diameter) (Fig. 4). In typical microelectronic production where Ø = 25 μm Al wires are used, the foot length is less than 50 μm, no groove is used, the front and back radii are roughly 25 μm, and the wire deformation may reach 60%.

In microelectronic products, the bond pads are often small (less than 150 μm side length). Therefore a long wedge foot can not be used, whereas in the wire-to-wire bonding the extent of the bonding spot is practically unlimited. The destructive pull test is optimized to produce less than 10% lifted bonds because a lifted bond causes a catastrophic failure in a typical microelectronic production setting. This goal is achieved by using process parameters that produce large wire deformation but also slightly reduce the average maximum sustainable pull force of the bonds. In comparison, a lifted bond in the tether production is not a catastrophic failure, rather an event comparable to a wire cut by a micrometeoroid.

Figure 14 shows the maximum sustainable pull force of 252 bonds along the 97 m post production tether. The measurement series started with a cleaned wedge. The build-up of Al contamination of the wedge causes the maximum sustainable pull force to drop to 90 mN after the first 8000 bonds. The last two measurements, marked by red diamonds, were measured after a second wedge cleaning. The important feature is that this cleaning returned the maximum sustainable pull force to the initial level.

The destructive pull test shows that during the 97 m test production (9700 bonds) the maximum sustainable pull force of the bonds was on average (99 ± 8) mN whereas the minimum value was 80 mN. The average value is more than six sigma above the required 50 mN pull force limit. In practice this means that those bonds that are attached after the wire-to-wire bonding process very likely exceed 50 mN limit. It also means that if the wedge is clean, the lifted bonds encountered during tether production can not be explained by normal variations in maximum sustainable pull force. Instead the failure mechanism for the lifted bonds differs from the failure mechanism produced by the pull test.

The bond is pulled along the base wire in the destructive pull test that simulates the centrifugal pull in space (Fig. 7(II) & 15c). In comparison, the wedge is retracted nearly perpendicular to the base wire after the bonding process (Fig. 9 & 15). The friction between the wedge and the wire as well as the orthogonal pull direction creates a stress concentration in the bond that therefore may be lifted even though the same bond previously may have passed the destructive pull test. The stress in the destructive pull test is less

concentrated thus allowing the bond sustain a larger pull force compared to the pull induced by the wedge. This difference in failure mechanisms explains why the number of lifted bonds during the 1 km tether production exceeds the number of failures predicted by the destructive pull test.

A single failed bond is seen in Fig. 9b below the wedge (E). The wire is curved under the wedge which indicates that the bond was not initially broken, but rather was peeled/lifted off when the wedge retracted, see Fig. 15(b).

Wedge contamination plays at least two roles in reducing tether quality. The contaminated aluminum at the edge of the groove (Fig. 6c) deforms the neck of the bond which reduces the bond's pull strength. Secondly, contamination in the wedge holes (Fig. 6d) increases the friction of the wire when the wedge is retracted. This friction increases the probability that the bond is lifted. This behavior is evident in Fig. 13 where the rate of failed and repaired bonds is reduced by the wedge cleanings.

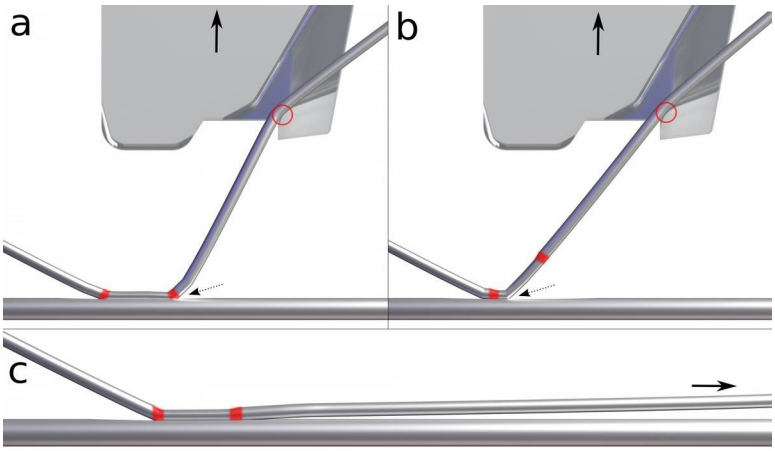

Figure 15. Schematic figure of a good (a) and failing (b) bond after wedge retraction. The wedge retraction pulls (arrow) the bond nearly perpendicular to the base wire (cfr Fig. 9) which induces high stress at the edge of the bond (dotted arrow). If the friction in the wedge (red circle) increases due to contamination and/or if the bond interface was poorly welded the bond may peel of and lift (b). In a destructive pull test, that simulates the centrifugal force felt by the E-sail after a base wire cut (cfr Fig. 7), the bond is pulled (arrow) along the base wire (c). In such a case the stress is less concentrated and the bond can sustain a higher pull force than in the previous case. The bond necks are highlighted in red (cfr Fig. 4).

4.2.2. 4-WIRE TETHER

Figure 11 shows a multifilament 4-wire tether. This post production tether was photographed right after the 1 km tether production and the structure is similar to the structure of the 1 km tether. This photo shows that the multifilament 4-wire Heytether can be produced using a 50 µm base wire and three 25 µm loop wires. The photo also shows the limitations of the manufactured tether. To improve the micrometeoroid tolerance the preferred Heytether design, Fig. 7(I), features variations in loop heights which are missing in the produced tether. The implemented 3-wire wedge (Fig. 5 & 6) enabled 4-wire tether production using a single wire bonder but removed the option of producing loops of different heights. Additionally the wire bonder limited the maximum loop height to 8 mm. Based on Eq. (3) and (5) the estimated tallest loops of the preferred Heytether should be at least 15 mm high. Lastly, Fig. 11 shows

the steep curve of the loop wires at the bond necks. This steepness is created by the bonder that retracts the wedge immediately after the bonding process as shown in Fig. 9(a) and 15(a). Figure 4 shows a detailed image of the bond neck. Due to the fragility of aluminum, the steep bending of the neck should be limited to avoid fatigue failure of the wire.

4.2.3. 1 KM TETHER QUALITY

Table 2 and Fig. 13 summarize the failed and repaired bonds during the 1 km tether manufacturing. Out of 90 704 produced bonds in 1 km tether 82 (0.1%) bonds or loops remained failed. Altogether 195 (0.2%) failures during the production were repaired. The number and cause of failures, repaired bonds, loop wire and base wire cuts were recorded during the production. In addition each image of a bond was analyzed post production to verify the obtained numbers.

The original target in the ESAIL EU project was to have less than 1% failed bonds. While the actual production clearly exceeded the target the measured failure rate is still far from those reported in the field of microelectronic wire bonding (< 0.002%) [17]. In practice the difference means that the wire-to-wire bonding process has potential to improve.

Table 2 identifies bond failures and failure modes. The failure mode actually indicates failures that either were visible after the bonding machine stopped or failures recorded based on the images of bonds. While the majority of the failures are categorized as lifted bonds the cause for the lifted bon ds is uncertain. While the most likely reason for the lifted bonds is lift-off caused by the wedge (Fig. 15(b)) we can not exclude other possibilities such as a misaligned wedge or loop wire, or a poorly clamped base wire.

The wire-to-wire bonding process requires accurate wire alignment of both the base wire and the loop wires because the loop wire should be bonded onto the center of the base wire to reach high quality. The custom built 3-wire wedge and base wedge were designed to give extra support for the wires during the bonding process. However, despite the efforts some of the lift-offs may be due to poorly aligned loop wires or to a base wire that was loose in the base wedge groove. The bonding spot width is approximately 5 μm (Fig. 4).

Wedge groove contamination, Fig 6(c), may reduce the stiction between the wedge and the wire. It may also reduce the capability of the wedge to align the wire and it may weaken the wire neck. The contamination is aluminum that has attached from the wire during the ultrasonic bonding. The pull test result in Fig. 14 indicates that contamination may reduce the average maximum sustainable pull force by 20 mN after 70 m tether production. During the 1 km tether production the average failure rate was 0.06% right whereas after wedge cleaning it was on average only 0.1%. Wedge cleaning removes the contamination and restores the wedge to its original state as shown by the last two measurements in Fig 14.

Figure 12 shows the 1 km tether on a production reel. The photo shows that reeling the tether is possible, even though testing and development is needed to ensure minimal tether defects during reel-in, storage and launch, as well as reliable deployment in space [56]. The aspects of tether reeling and deployment are outside the scope of this thesis.

4.3. E-sail tether production outlook

The produced 1 km tether was the first of its kind. While it proves that the E-sail tether can be produced on km scale, it is evident that the tether development has not reached its end. To build a full scale E-sail and to use it as a propulsion method in an interplanetary mission, improvements in tether production speed, tether topology, wire-to-wire bonds, tether reeling and testing are needed.

4.3.1. Improvements to wire-to-wire bonding

The wire-to-wire bond quality fulfills the desired requirements. However, improvements in wedge material and shape, as well as loop shape could improve the bond pull strength and long term reliability, and reduce the number of failures during tether production.

Based on our results, the wedge contamination reduces the pull strength of the wire-to-wire bond and increases the failure rate in tether production. To improve the situation, new wedge materials should be studied. For example ceramic wedges, used in thermosonic wire bonding, withstands regularly over 1 000 000 bonds without cleaning [57]. That would correspond to producing a 30 km long tether without cleaning.

The wedge retraction path could be improved. Instead of lifting perpendicularly to the base wire, the wedge could move at an angle that allows wire transition inside the wedge with minimum friction. In Fig. 15(a), the angle would be 45 degrees. Alternatively the base wire spooling could be synchronized with the wedge retraction to produce the same effect.

The wedge has proved to produce bonds with high maximum sustainable pull force. However, the neck shape could be improved to ensure long term reliability of the wire-to-wire bond. Currently, if the loop is pulled/pushed the wire bends at the neck making the neck act like a hinge. Since the Al-wire can not withstand repetitive bending, the loop wire may break at the neck during spooling, transportation, launch vibrations, deployment or operation. To reduce this probability the transition of the bond (wire) to the loop (wire) at the neck should be as smooth as possible. A smooth neck lets the wire bend in larger radius and minimizes strain aging in the neck. The smooth neck could be produced by having even larger front and back radii in the wedge foot and by adjusting the groove shape in such a way that the wire is not deformed horizontally during the bonding process. An example of a bond made with such a groove shape is in ref. [17] Figure 2-16.

4.3.2. Improvements for tether production

The proposed full scale 1 Newton E-sail features one hundred 20 km long tethers. Whereas the production rate during our 1 km tether manufacturing was 70 m/24 h, or 11 s/bond, it could in principle be improved to at least 400 m/day, i.e., 2 s/bond. This conservative estimate may be compared with the performance of commercial wire bonders that produce more than 10 bonds/s (wire to pad). With a 400 m/day production rate a full scale (20 km long) E-sail tether could be produced in 50 days. To simplify the programming, the tetherfactory and bonder operated previously mostly in serial mode, where each operation had its own time slot (see paper [II] online video). By applying parallel operations and reducing dwell times between operations the estimated 2 s/bond with the existing device is feasible (Fig. 16).

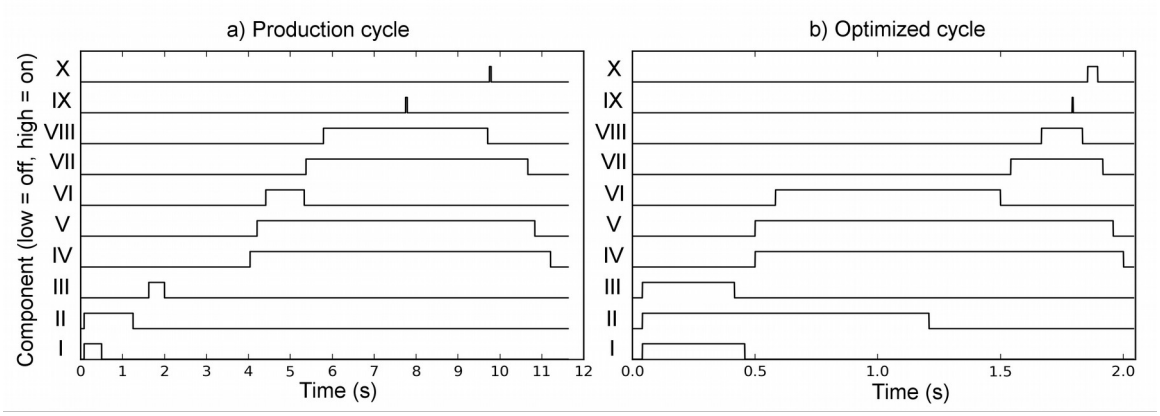

Figure 16. Time-line of tether production cycles. a) Production cycle used in the 1 km tether production and b) Optimized cycle to show that by reducing idling and applying parallel operations a single loop can be produced in 2 seconds using the existing tetherfactory. The components/actions are I) tether reel, II) tetherfactory alignment, III) reel alignment, IV) clamp, V) tension, VI) flattening, VII) loop forming pin, VIII) wedge, IX) ultrasonic bond and X) optical inspection. The cycle is visualized in a multimedia presentation included in the online files of paper II.

The tether topology (shape) needs to be improved for the E-sail mission. The Heytether shape with different loop heights (Fig. 7(I)) is needed to achieve the necessary micrometeoroid tolerance. It could be achieved by a multi-head bonder and/or improved wire controlling mechanism. An illustration based on MSc. Timo Rauhala's idea of three consecutive bonders is shown in Fig. 17. The illustration is a source for inspiration rather than a finalized design of the production machine.

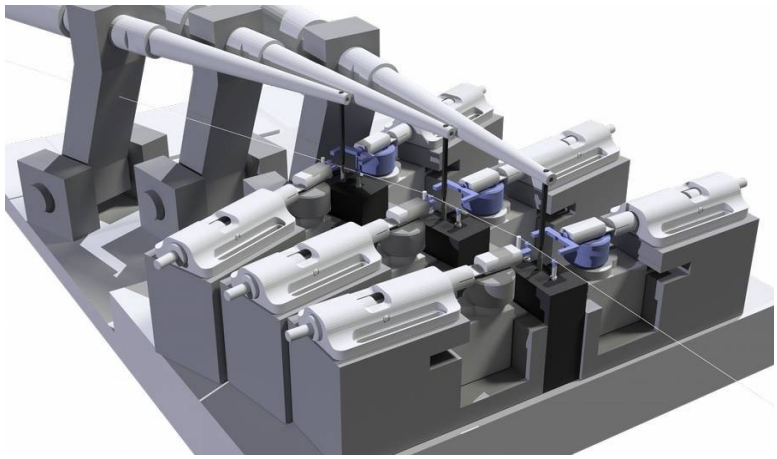

Figure 17. Illustration of a tetherfactory with three bond heads.

4.3.3. Online quality measurements

We used an optical microscope camera to measure whether the bond lifted during the 1 km tether manufacturing. However, it could be beneficial to be able to predict the bond strength of each bond during production. This would permit one to rank the overall tether quality. A high-quality tether would have strong bonds and few failed bonds. Higher assured tether (bond) strength would enable higher E-sail rotational speed and/or longer tethers which would increase the propulsion/mass ratio of the E-sail.

Increasing this ratio would improve the competitiveness of the E-sail technology since it increases the payload and/or shortens the transit time to its destination.

Based on the results of this thesis the improved online quality control system should be able to detect at least 1) bonds that are going to lift, 2) need for the wedge cleaning, and 3) stuck/displaced wires.

Methods exist that could non-destructively predict the wire-to-wire bond strength [V, VIII, 32]. Another option is to measure the bonding process in real-time to probe anomalies and therefore detect potentially bad bonds [22, 58–60]. The latter methods could even predict the bond quality during the bonding process and tune (in real-time) the process parameters to ensure high quality bonds [29, 61]. Additionally, a sensitive force sensor could measure the tension of the wire during wedge retraction to detect the need for wedge cleaning whereas a camera could detect the stuck/displaced wires.

Even if the improved wedge (ceramic) and wire handling mechanics in the tether factory significantly could reduce the number of wire-to-wire bond failures in future tethers, the need for the online wire-to-wire bond quality control hardly disappears. The reason is simple; it is difficult to replace a failed tether in space.

4.4. Conclusions

Tethers are a key element of the electric solar wind sail (E-sail). This thesis claims that it is possible to manufacture E-sail tether on km scale. To prove the claim we produced 1.04 km long 4-wire multifilament tether out of Ø = 25 μm and Ø = 50 μm aluminum wires. The tether comprises 90 704 wire-to-wire bonds and a bonding yield of 99.9% was achieved. This 1 km tether was the most important objective of the ESAIL EU FP7 -framework project.

References

1. P. Janhunen, Electric sail for spacecraft propulsion. *Journal of Propulsion and Power*. **20**, 763 (2004).

2. D. R. Williams, Chronology of Lunar and Planetary Exploration, National Space Science Data Center (NSSDC), available at http://nssdc.gsfc.nasa.gov/planetary/chronology.html. (Accessed 2014-09-08).

3. R. Saunders, NASA's Solar System Exploration Program. American Institute of Aeronautics and Astronautics, (2000-09-19).

4. I. De Pater, *Planetary sciences* (Cambridge University Press, Cambridge ; New York, 2001).

5. J. J. Lissauer, *Fundamental planetary science: physics, chemistry, and habitability* (Cambridge University Press, New York, NY, USA, 2013).

6. A. A. Quarta, G. Mengali, P. Janhunen, Optimal interplanetary rendezvous combining electric sail and high thrust propulsion system. *Acta Astronautica*. **68**, 603–621 (2011).

7. A. A. Quarta, G. Mengali, Electric Sail Mission Analysis for Outer Solar System Exploration. *Journal of Guidance, Control, and Dynamics*. **33**, 740–755 (2010).

8. G. Mengali, A. A. Quarta, Non-Keplerian orbits for electric sails. *Celestial Mechanics and Dynamical Astronomy*. **105**, 179–195 (2009).

9. J.-M. Siguier *et al.*, Drifting Plasma Collection by a Positive Biased Tether Wire in LEO-Like Plasma Conditions: Current Measurement and Plasma Diagnostic. *IEEE Transactions on Plasma Science*. **41**, 3380–3386 (2013).

10. Pekka Janhunen, Coulomb drag devices: electric solar wind sail propulsion and ionospheric deorbiting. Space Propulsion 2014, Köln, Germany, (19-22 May 2014).

11. P. Janhunen, Increased electric sail thrust through removal of trapped shielding electrons by orbit chaotisation due to spacecraft body. *Ann. Geophys.* **27**, 3089–3100 (2009).

12. Hannu Koivisto, Taneli Kalvas, Pekka Janhunen, Tether space environment requirements. EU FP7 ESAIL deliverable D23.1, (2011).

13. P. Janhunen, A. Sandroos, Simulation study of solar wind push on a charged wire: basis of solar wind electric sail propulsion. Annales Geophysicae. 25, 755–767 (2007).

14. E. Grün, H. A. Zook, H. Fechtig, R. H. Giese, Collisional balance of the meteoritic complex. *Icarus*. **62**, 244–272 (1985).

15. Robert L. Forward, Robert P. Hoyt, Failsafe Multiline Hoytether Lifetimes. 1st AIAA/SAE/ASME/ASEE Joint Propulsion Conference, *paper 95-28903,* San Diego, CA, (1995).

16. R. P. Hoyt, R. L. Forward, Alternate interconnection hoytether failure resistant multiline tether. United States Patent: 6286788, (2001).

17. G. Harman, *Wire Bonding in Microelectronics: Materials, Processes, Reliability, and Yield* (McGraw-Hill

Professional, ed. 2, 1997).

18. J. E. Krzanowski, N. Murdeshwar, Deformation and bonding processes in aluminum ultrasonic wire wedge bonding. *Journal of electronic materials*. **19**, 919–928 (1990).

19. G. Harman, J. Albers, The Ultrasonic Welding Mechanism as Applied to Aluminum-and Gold-Wire Bonding in Microelectronics. *Parts, Hybrids, and Packaging, IEEE Transactions on*. **13**, 406–412 (1977).

20. A. Shah *et al.*, Ultrasonic friction power during Al wire wedge-wedge bonding. *J. Appl. Phys.* **106**, 013503–8 (2009).

21. C. M. Hu, N. Guo, H. Du, W. H. Li, M. Chen, A microslip model of the bonding process in ultrasonic wire bonders Part I: Transient response. *The International Journal of Advanced Manufacturing Technology*. **29**, 860–866 (2006).

22. H. Gaul *et al.*, The ultrasonic wedge/wedge bonding process investigated using in situ real-time amplitudes from laser vibrometer and integrated force sensor. *Microelectronic Engineering*. **87**, 537–542 (2010).

23. H. Gaul, M. Schneider-Ramelow, H. Reichl, Analysis of the friction processes in ultrasonic wedge/wedge-bonding. *Microsystem Technologies*. **15**, 771–775 (2009).

24. Henri Seppänen *et al.*, Nanoscale bonding. IMAPS Topical Workshop & Tabletop Exhibition on Wire Bonding, San Jose, CA, USA, (2014).

25. G. Harman, C. Cannon, The Microelectronic Wire Bond Pull Test-How to use It, How to Abuse It. *IEEE Transactions on Components, Hybrids, and Manufacturing Technology*. **1**, 203– 210 (1978).

26. MIL-STD-883H, Department of Defence, USA, (2010).

27. G. G. Harman, Metallurgical Failure Modes of Wire Bonds. 12th Annual Reliability Physics Symposium, pp. 131–141, (1974).

28. MIL-PRF-38535H, Department of Defence, USA, (2007).

29. S. Hagenkotter, M. Brokelmann, H.-J. Hesse, PiQC - a process integrated quality control for nondestructive evaluation of ultrasonic wire bonds. Ultrasonics Symposium, (IUS, IEEE), pp. 402–405, (2008).

30. S. W. Or, H. L. W. Chan, V. C. Lo, C. W. Yuen, Ultrasonic wire-bond quality monitoring using piezoelectric sensor. *Sensors and Actuators A: Physical*. **65**, 69–75 (1998).

31. R. Gilardoni, S. Hagenkötter, M. Brökelmann, Process Integrated Quality Control for Wire Bonding. IMAPS 2008 The 41st International Symposium on Microelectronics, (2008).

32. K. K. Sreenivasan, M. Srinath, A. Khotanzad, Automated vision system for inspection of IC pads and bonds. *Components, Hybrids, and Manufacturing Technology, IEEE Transactions on*. **16**, 333–338 (1993).

33. D. D. J. Evans, Geometry and Bond Improvements for Wire Ball Bonding and Ball Bumping. IMAPS, (8 - 12 October 2006).

34. A. E. Carpenter *et al.*, CellProfiler: image analysis software for identifying and quantifying cell phenotypes. *Genome Biol.* **7**, R100 (2006).

35. R Core Team, R: A language and environment for statistical computing. R Foundation for Statistical

Computing, Vienna, Austria. ISBN 3-900051-07-0, (2012).

36. C. A. Schneider, W. S. Rasband, K. W. Eliceiri, NIH Image to ImageJ: 25 years of image analysis. *Nat Meth*. **9**, 671–675 (2012).

37. G. Mengali, A. A. Quarta, P. Janhunen, Electric Sail Performance Analysis. *Journal of Spacecraft and Rockets*. **45**, 122–129 (2008).

38. TRL Handbook, ESA, TEC-SHS/5551/MG/ap, issue 1 revision 6 (September 2008).

39. Bruce Wiegmann, Heliopause Electrostatic Rapid Transit System (HERTS) (2014), available at http://www.nasa.gov/content/heliopause-electrostatic-rapid-transit-system-herts/#.VA2iHx9th5E, (accessed 2014-09-08).

40. Pekka Janhunen, Final Report, ESAIL FP7-CP, 262733, (2010-2013).

41. P. Janhunen, Electrostatic Plasma Brake for Deorbiting a Satellite. *Journal of Propulsion and Power*. **26**, 370–372 (2010).

42. S. Lätt *et al.*, ESTCube-1 nanosatellite for electric solar wind sail in-orbit technology demonstration. *Proceedings of the Estonian Academy of Sciences*. **63**, 2000 (2014).

43. O. Khurshid, T. Tikka, J. Praks, M. Hallikainen, Accommodating the plasma brake experiment on-board the Aalto-1 satellite. *Proceedings of the Estonian Academy of Sciences*. **63**, 258 (2014).

44. Anni Toppila *et al.*, Space Tether Produced to Strength Specification, International Ultrasonics Symposium (IUS), Prague, Czech Republic, (2013).

45. Göran Maconi *et al.*, Determining the Quality of Space Tether in a Nondestructive manner, International Ultrasonics Symposium (IUS), Prague, Czech Republic, (2013).

46. Henri Seppänen *et al.*, Multifilament Tether for Electric Solar Wind Sail, IMAPS Workshop on Wire Bonding, San Francisco Marriott Hotel, San Francisco, CA, (2011).

47. M. Oinonen *et al.*, ALICE Silicon Strip Detector Module Assembly with Single-Point TAB Interconnections, Proceedings of the Conference LECC, Heidelberg, Germany, (2005).

48. H. Seppänen, A. Kaskela, A. Wallin, M. Oinonen, E. Hæggström, Laser Doppler vibrometer measurements to verify microslip model of the bonding process. Proceedings of the International Congress on Ultrasonics, Vienna, Paper ID 1423, (9-13 April 2007).

49. Timo Rauhala *et al.*, Automatic 4-wire Heytether production for the Electric Solar Wind Sail. IMAPS Wire Bonding Workshop, (23 Jan 2013).

50. Zoran Radivojevic, Ivan Kassamakov, Markku Oinonen, Pasi Vihinen, Henri Seppänen, IR thermography for quality assessment of microelectronic devices. Proceedings of 7th Conference on Quantitative Infrared Measurements (2004).

51. V. Heikkinen *et al.*, Quality control of ultrasonic bonding tools using a Scanning White Light Interferometer. Ultrasonics Symposium (IUS), IEEE, pp. 1428–1430, (2010).

52. R. Kurppa *et al.*, Real-Time Nondestructive Contact Resistance Method to Estimate Wire Bond Pull Force,

Review of Progress in Quantitative Nondestructive Evaluation Volume 29, pp. 1601–1608, (2010).

53. H. Seppänen *et al.*, Scanning white light interferometry in quality control of single-point tape automated bonding. Photonics North 2004, SPIE, Ottawa, Canada, vol. 5578, pp. 519–526, (2004).

54. Z. Radivojevic *et al.*, Transient IR imaging of light and flexible microelectronic devices. *Microelectronics and Reliability*. **46**, 116–123 (2006).

55. H. Seppänen, A. Kaskela, K. Mustonen, M. Oinonen, E. Haeggstrom, Understanding Ultrasound-Induced Aluminum Oxide Breakage During Wirebonding. Ultrasonics Symposium, IEEE, pp. 1381–1384, (2007).

56. Timo Rauhala, Göran Maconi, Main tether reel test results. EU FP7 ESAIL deliverable D32.4, (2013).

57. Rich Rice, KEYNOTE: The Way Forward for Wirebond Packaging. Topical Workshop & Tabletop Exhibition on Wire Bonding, IMAPS, (2014).

58. M. Brökelmann, J. Wallaschek, H. Hesse, Bond process monitoring via self-sensing piezoelectric transducers. Frequency Control Symposium and Exposition, Proceedings of the 2004 IEEE International, pp. 125–129, (2004).

59. M. Mayer, J. Schwizer, Microelectronic Bonding Processes Monitored by Integrated Sensors. *Sensors Update*. **11**, 219–277 (2002).

60. J. Grigoraschwili, W. Scheel, M. Thiede, Charakterisierung von Ultraschall-Schweißverbindungen durch Messen des elektrischen Durchgangswider- stands. *Schweißtechnik*. **34**, 468–470 (1984).

61. H. Gaul, M. Schneider-Ramelow, K. D. Lang, H. Reichl, Predicting the Shear Strength of a Wire Bond Using Laser Vibration Measurements. Electronics Systemintegration Technology Conference, IEEE, vol. 2, pp. 719–725, (2006).

Appendix A. A Short History of The Tetherfactory

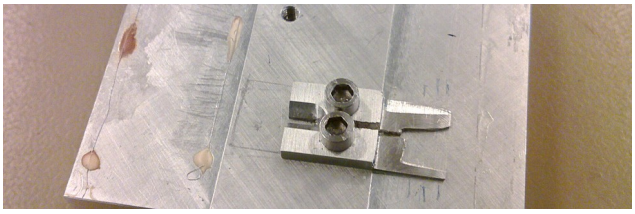

Figure 1. A jig to produce first wire-to-wire bonds without gluing the base wire onto the substrate. (2007)

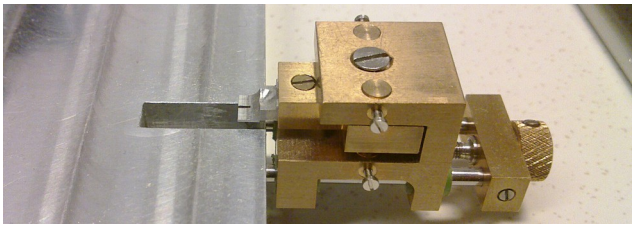

Figure 2. A jig to test base wire clamping and wire-to-wire bonding. (3/2009)

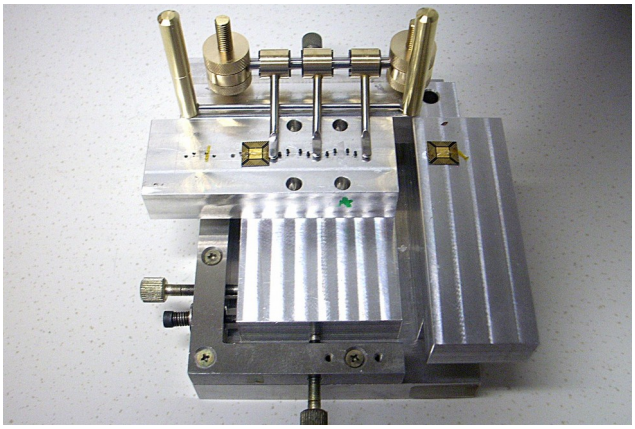

Figure 3. A test jig with the tension arms for testing single loop bonding. (6/2009)

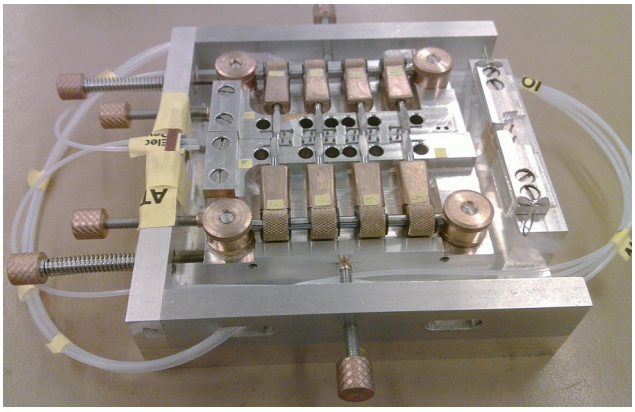

Figure 4. A tetherfactory for continuous 4-wire Hoytether production. (8/2009)

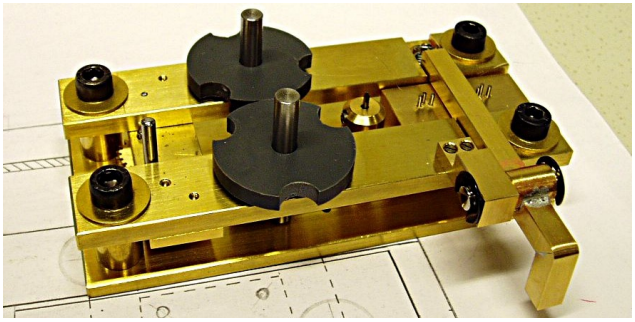

Figure 5. A tetherfactory for 2-wire Heytether production. The wire-to-wire bonds were produced over the base wedge. (2/2010)

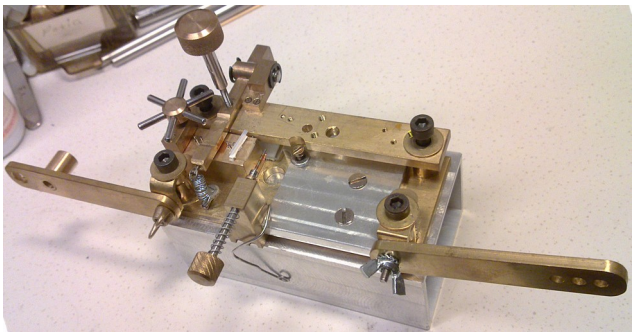

Figure 6. A tetherfactory for 2-wire Heytether production. The base wire was clamped by a manually operated clamp and tension was created by a tension arm. A pin helped to form the loops. (3/2010)

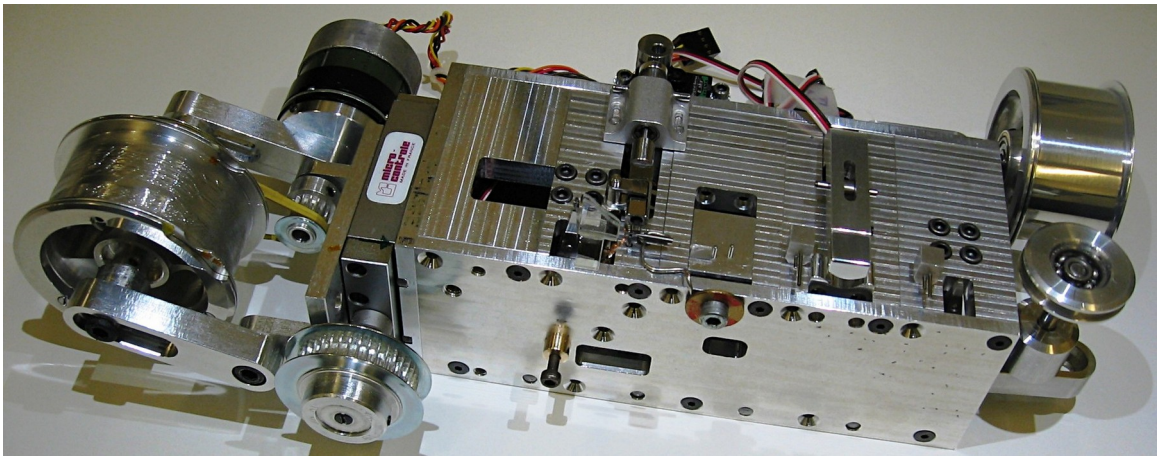

Figure 7. The first version of the automatic tetherfactory. The modified version of this device was eventually used to produce 1 km long 4-wire tether. (8/2011)